

Control Algorithm for Non-isolated Supercapacitor Based Kinetic Energy Recovery System

Luka Lopin¹, Slobodan Vukosavić² and Nikola Lepojević²

1. Computer Controlled Systems, Lola Institute, Belgrade 11030, Serbia

2. The Department of Power Converters and Drives, University of Belgrade, Belgrade 11120, Serbia

Abstract: This paper presents the control algorithm for supercapacitor based kinetic energy recovery system. Supercapacitor shares energy with the motor drive DC link through bidirectional non-isolated converter. Two cascaded linear regulators control feedback linearized states of the system. As a result, the DC link voltage is stabilized and the supercapacitor voltage and current are limited. Control algorithm does not increase ripple of voltages and currents, and thus life time expectancy of supercapacitor is prolonged. In torque-controlled motor drives, current on DC side can rapidly change with bandwidth as high as 2 kHz. Based on measurements of KERS states, the algorithm estimates rapidly changing motor drive current on DC side and stabilizes the DC link voltage with overshoot less than 2%. Controller is independent from the motor drive parameters and relies only on its own measurements. This enables kinetic energy recovery system (KERS) to be a standalone device.

Key words: Supercapacitor KERS, energy storage, regenerative braking, energy recovery, control system.

1. Introduction

There are two types of supercapacitors (SC); pseudocapacitor and electric double layer capacitor (EDLC) [1]. Emerging energy storage unit for power applications are EDLC [2]. EDLC consists of two nanoporous active carbon electrodes with specific surface area in range of 1,000-2,500 m²/g [3]. Such capacitors have specific capacitance in range of 100-200 F/g [4]. SCs have approximately one hundred time greater energy density than electrolytic capacitor and ten time greater power densities than chemical batteries [5] and high life time expectancies—up to 10 years [6]. This makes SCs a promising device for energy storage applications.

There is a need for braking in the motor drive systems. Motor drives most commonly break via dynamic braking resistor (DBR). While braking, the electric machine changes from motor to generator regime [7]. Kinetic energy of the shaft is than transformed into electric energy and it's transferred to

the DC link of the electric drive. As a consequence, DC link voltage increases above nominal value. At this moment, switch turns on DBR and irreversibly dissipates excess of energy to heat. Fig. 1 shows topology of motor drive with the DBR.

Kinetic energy of a drive could be recuperated via active rectifier. But for end user, such recuperation is same as if no energy is recuperated, since energy companies in most countries are not paying for intermittent bursts of energy.

SC based kinetic energy recovery system (KERS) transfers energy from the DC link to the SC through bidirectional converter during braking. Later, during acceleration, braking energy is recovered from the SC to the DC link and consequently to the electric machine. Topology of motor drive with the KERS is shown on Fig. 2. Same KERS topology is used in Refs. [8-15].

Control algorithm of KERS is expected to fulfill following basic tasks:

- Charging SC while motor drive is braking;
- Discharging SC while motor drive is accelerating;
- Limiting voltage and current of SC;
- Stabilizing DC link voltage.

Corresponding author: Luka Lopin, M.A., research fields: signals and systems.

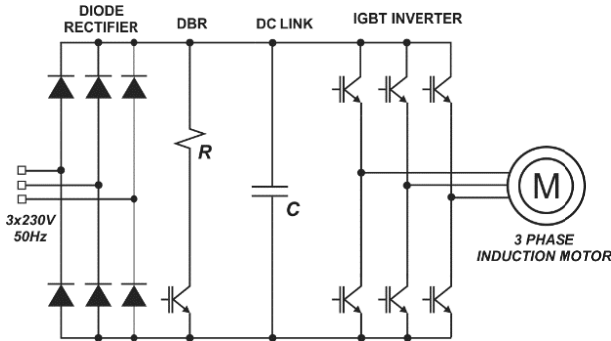


Fig. 1 Motor drive topology with DBR.

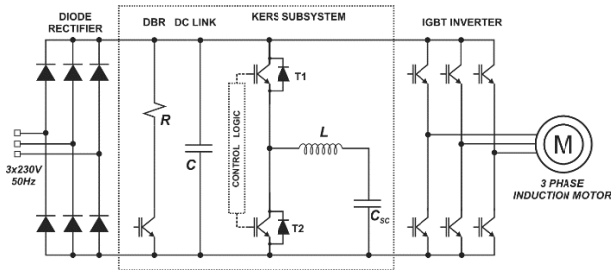


Fig. 2 Motor drive topology with SC based KERS.

Achieving these tasks is followed by certain difficulties. Increased voltage and current ripple can lead to irreversible degradation of SC [5] and consequently to shorter MTBF of a KERS. While ripple of current and voltage is inherent for the circuit in Fig. 2 due to switching operation of the transistors T_1 and T_2 , it is of interest not to further increase ripple by applying inadequate control algorithm. Such algorithm increases ripple due to local instabilities in the regulator. Instabilities are result of a nonlinearity of the controlled system or a change of the system parameters.

In Refs. [8-9] modified linear controller is proposed. In Ref. [8] SC current ripple reaches 10% and system has low closed loop bandwidth because of PLL. In Ref. [9] regulator relies on two aging sensitive parameters—capacitance of DC link and SC. Thus it requires occasional tuning of parameters. In Refs. [10, 11] fuzzy logic controller is proposed. In Ref. [10] SC current ripple is slightly improved compared to classic controllers and it reaches 25% in the worst case. In Ref. [11], controller depends on motor drive measurements. The ripple is greatly improved, but controller requires occasional fine tuning. In Refs. [12, 13] neural

networks are proposed for energy management of SC in hybrid vehicles. In Refs. [14, 15] flatness and passivity based control are proposed. Controllers are dependent on aging sensitive parameters of DC link and SC capacitance.

The aim of this paper is to devise a novel control algorithm able to achieve basic tasks of KERS with improved ripple, robustness and closed loop bandwidth. This paper proposes feedback linearization based controller with estimation of motor drive current.

2. Control Strategy

Control algorithm stabilizes the DC link voltage, while limiting SC voltage and current. General control block diagram is shown in Fig. 3. Inner loop controls the SC current. Output of inner regulator controls transistors T_1 and T_2 using the PWM method. In Refs. [8-13] all algorithms comprise of inner current controller. Outer loop controls DC link voltage. Outer regulator output represents the SC current reference. The current reference is dynamically limited to ensure proper limiting of the SC voltage.

Upper and lower SC current limits depend on SC voltage. Similar dynamic current limits are utilized in Ref. [12]. Current limits, for current direction as in Fig. 5, are as follows:

- If $U_{sc} \in [U_{min}, U_{max}] \Rightarrow i^* \in [-I_{max}, I_{max}]$
- If $U_{sc} > U_{max} \Rightarrow i^* \in [0, I_{max}]$ and DBR is on
- If $U_{sc} < U_{min} \Rightarrow i^* \in [-I_{max}, 0]$ and KERS is off

The DC link voltage reference is fixed slightly above the maximum voltage of the diode rectifier. This method is used in Ref. [8]. If regulator manages to stabilize the DC link voltage, diode rectifier is inversely polarized and energy exchange occurs only between the motor drive and the SC. As long as the voltage of the SC is in segment $U_{sc} \in [U_{min}, U_{max}]$ and motor drive power is less than KERS unit maximum power, regulator will be able to keep the DC link voltage at the reference point. This enables KERS system to completely discharge energy of the SC during acceleration with a rate dictated by the motor drive.

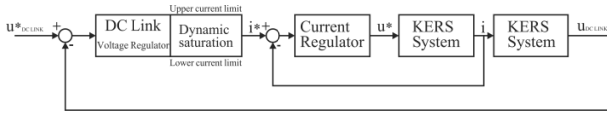


Fig. 3 General control block diagram of KERS.

When SC voltage is at the minimum value, current reference limits are changed to prevent further discharge of the SC. The DC link voltage drops to the nominal value, diode rectifier turns on and the KERS unit turns off. When SC voltage is at the maximum value, current reference limits are changed to prevent further charging of SC and DBR is turned on to prevent dielectric rupture of the DC link.

Often, SCs are used to recover part of kinetic energy. If the braking torque of the motor drive is too large, the DC link voltage will increase regardless of the KERS unit transferring energy with maximum current to the SC. At this moment, the DBR should be turned on. In such scenario, the DC link voltage is limited by DBR action and part of the shaft's kinetic energy is recovered in KERS unit.

During acceleration of motor drive, the DC link voltage tends to decrease. If accelerating torque of the motor drive is too large, the DC link voltage will decrease regardless of the KERS unit transferring energy with maximum current from the SC to the DC link. At one moment, the DC link voltage drop will be sufficient to turn on the diode rectifier. Now motor drive is jointly powered from the KERS unit and the diode rectifier. The KERS regulator is unsuccessfully trying to increase the DC link voltage to the reference value with maximum SC current, thus draining the SC voltage to the minimum value. Once SC is drained, KERS unit turns off.

3. Control-Oriented KERS Modeling

For the purpose of regulator synthesis, rectifier's and inverter's influence on the DC link are modeled as disturbance current. Such circuit is shown in Fig. 4. This current acts as a disturbance on DC link voltage.

There are several models of SC ranging from non-linear model [16], RC network model [17] and

simple RC model. For the purpose of regulator synthesis, such models are inadequate. Modeling SC as RC circuit has certain difficulties. It is impossible to neglect combined resistance of inductor and SC internal resistance. Great capacitance of SC results in real poles of the LRC_{sc} network and poles of the LC_{sc} network are imaginary. SC capacitance and internal resistance are aging sensitive. This fact combined with aging sensitive DC link capacitance results in serious deterioration of regulator robustness over time.

One should notice SC's dynamics are several decades slower than dynamics of inductor and DC link. Over several sampling periods of regulator, SC voltage is roughly constant. For the reason of increasing robustness of KERS unit, SC is modeled as ideal voltage source. Voltage of SC is measured and updated in each sampling period of regulator. Fig. 5 shows circuit with SC modeled as constant voltage source and rectifier and inverter modeled as disturbance current.

State space model of circuit shown in Fig. 5 can be written as Eq. (1) and Eq. (2), where:

- I_d —inverter and rectifier modeled as current disturbance;
- E —SC modeled as constant voltage source;
- L —inductor's inductance;
- C —DC link capacitance;
- i —inductor's current, also SC's current;
- u_c —DC link capacitor voltage;

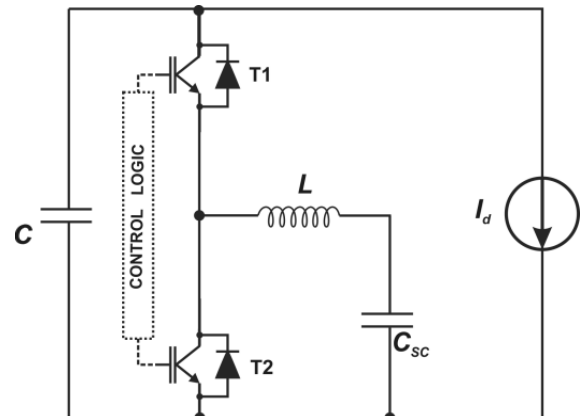


Fig. 4 KERS circuit with inverter and rectifier modeled as current disturbance.

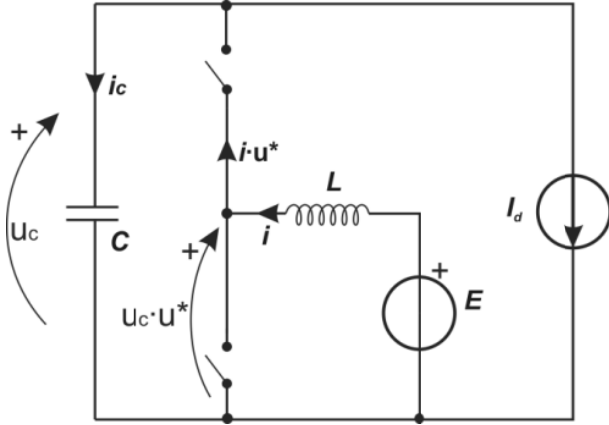


Fig. 5 KERS circuit with inverter and rectifier modeled as current disturbance and SC modeled as constant voltage source.

• u^* —control signal representing duty ratio of PWM controlled transistors; $u^*=1$ —upper switch is on (T1 on Fig. 2); $u^*=0$ —lower switch is on (T2 on Fig. 2); $u^* \in [0,1]$ and $u^* \in R$

$$\frac{di}{dt} = \frac{E}{L} - \frac{u_c}{L} u^* \quad (1)$$

$$\frac{du_c}{dt} = -\frac{1}{C} I_d + \frac{i}{C} u^* \quad (2)$$

This model describes dynamic of inductor and DC link. SC dynamic is neglected on purpose. Model has four parameters. SC voltage E and disturbance current I_d are measurable. Inductance L is stable parameter. Parameter C is aging sensitive parameter. DC link usually consists of electrolytic capacitor. Its capacitance degrades in time and decreases robustness of regulator.

4. Disturbance Current I_d Estimation

High performance position controlled systems usually consist of inner torque control loop. Position is controlled by applying maximum torque for braking and acceleration. In such systems, inverter's current on DC side can change from maximum positive current to maximum negative current in 0.5 ms [18]. Therefore, influence of disturbance current is crucial and simple feedback DC link voltage regulator is not sufficient to stabilize voltage during intermittent mode of motor drive.

During operation of interest, diode rectifier is inversely polarized, and disturbance current equals inverter's current on DC side. Measuring disturbance current is not practicable. Current sensor increases price and hardware complexity. Measured current is pulsed and therefore noisy. No matter which filtering technique is utilized, noise remains and jeopardizes regulator's stability, hence increasing SC's current and voltage ripple and decreasing expected lifetime of SC.

Disturbance current could be estimated from Eq. (2) written as Eq. (3). Pulsed noise is significantly reduced and low noise signal is attained with simple low pass digital filter.

$$I_d = i \cdot u^* - C \frac{du_c}{dt} \quad (3)$$

Final form of disturbance current estimator is obtained by applying digital low pass filter on Eq. (3) with sampling period T coinciding sampling period of regulator and bandwidth frequency ω_1 , written as Eq. (4). Control signal u^* is delayed one sampling period to obtain causal estimator.

$$I_d^{estim} = \frac{1 - e^{-\omega_1 T}}{1 - z^{-1} e^{-\omega_1 T}} \cdot i \cdot u^* \cdot z^{-1} - C \frac{2\omega_1 - 2\omega_1 z^{-1}}{(\omega_1 T + 2) + (\omega_1 T - 2)z^{-1}} u_c \quad (4)$$

5. State Transformation and Feedback Linearization

Model of KERS unit described with Eqs. (1) and (2) is nonlinear. Because of very wide range of SC's voltage and current and bidirectional power flow, linear regulator will have regimes with increased current and voltage ripple. For this reason, some authors use modified linear controllers [8, 9], fuzzy logic regulators [10, 11], neural networks [12, 13] or flatness and passivity control theories [14, 15].

This paper proposes feedback linearization control method. Regulator synthesis consists of three steps:

- state transformation to utilize non-linear state space system in controllable canonic form;
- feedback linearization of transformed states;

- linear regulation of linearized states.

States i and u_c can be written in different notation, as in Eq. (5). Now system could be written as Eqs. (6), (7), (8) in vector form.

$$X = \begin{bmatrix} i \\ u_c \end{bmatrix} = \begin{bmatrix} x_1 \\ x_2 \end{bmatrix} \quad (5)$$

$$f(X) = \begin{bmatrix} \frac{E}{L} \\ -\frac{I_d}{C} \end{bmatrix} \quad (6)$$

$$g(X) = \begin{bmatrix} -\frac{x_2}{L} \\ \frac{x_1}{C} \end{bmatrix} \quad (7)$$

$$\dot{X} = f(X) + g(X) \cdot u^* \quad (8)$$

System in Eq. (8) is not in controllable canonic form. State transformed and feedback linearized target system in controllable canonic form is written as Eqs. (9) and (10) with transformed states z_1 and z_2 .

$$\dot{z}_1 = z_2 \quad (9)$$

$$\dot{z}_2 = v \quad (10)$$

Let's now introduce state z_1 in function of states x_1 and x_2 written as Eq. (11). First Lie derivative of Eq. (11) is written as Eq. (12).

$$z_1 = h(X) \quad (11)$$

$$\dot{z}_1 = L_f h(X) + L_g h(X) \cdot u^* \quad (12)$$

Equalizing Eqs. (9) and (12) we have Eqs. (13) and (14).

$$L_g h(X) = \begin{bmatrix} \frac{\partial h(X)}{\partial x_1} & \frac{\partial h(X)}{\partial x_2} \end{bmatrix} \begin{bmatrix} -\frac{x_2}{L} \\ \frac{x_1}{C} \end{bmatrix} = 0 \quad (13)$$

$$z_2 = L_f h(X) = \begin{bmatrix} \frac{\partial h(X)}{\partial x_1} & \frac{\partial h(X)}{\partial x_2} \end{bmatrix} \begin{bmatrix} \frac{E}{L} \\ -\frac{I_d}{C} \end{bmatrix} \quad (14)$$

Solving partial differential Eq. (13) and later Eq. (14) leads to transformed state system in controllable canonic form. State transformation is given with Eqs. (15) and (16).

$$z_1 = \frac{1}{2} L x_1^2 + \frac{1}{2} C x_2^2 \quad (15)$$

$$z_2 = E x_1 - I_d x_2 \quad (16)$$

Eq. (15) shows first transformed state z_1 is sum of energies of reactive components of KERS. Eq. (16)

shows second transformed state z_2 is sum of power of all sources and drains in KERS model.

System with partially transformed states in controllable canonic form is given with Eqs. (9) and (17).

$$\dot{z}_2 = \frac{E^2}{L} - \frac{I_d^2}{C} - \left(\frac{E}{L} x_2 + \frac{I_d}{C} x_1 \right) u^* \quad (17)$$

By defining control signal u^* as Eq. (18), system is feedback linearized from new control input v to transformed output states z_1 and z_2 and target system from Eqs. (9) and (10) is achieved.

$$u^* = -\frac{1}{\frac{E}{L} x_2 + \frac{I_d}{C} x_1} \left[-\frac{E^2}{L} + \frac{I_d^2}{C} + v \right] \quad (18)$$

6. Linear Regulator

Estimated disturbance current I_d and measured SC voltage E are not constant in time. Each sampling period I_d and E are updated and feedback linearization and state transformation output are altered. With I_d having ability to rapidly change from maximum positive to maximum negative value in 0.5 ms, process of updated feedback linearization and state transformation acts as a feedforward action on disturbance suppression of DC link voltage. With feedforward action, linear regulator can have single integral action. Proposed regulator is shown in Fig. 6. It comprises of inner PI regulator of state z_2 and outer P regulator of state z_1 .

Control object is double integrator. The control problem is analogous to position control of motor drives, thus similar controlling techniques could be used. In Ref. [19] optimal PID position controller is given. This paper proposes optimal PPI regulator with modeled computational delay and same optimization method as in Ref. [19].

To obtain optimal discrete PPI regulator, control object must be discretized. First integrator is written in

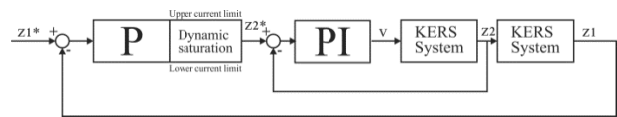


Fig. 6 Proposed PPI regulator of linearized KERS .

integral form as Eq. (19).

$$z_2(t - t_0) = z_2(t_0) + \int_{t_0}^t v(t) dt \quad (19)$$

PWM controlled converters are usually switched via IGBT transistors with frequencies in range of 10 kHz and higher. With such high frequencies, DSP brings computational delay of one sampling period. Computational delay alters closed loop dynamics and it has to be taken into account. Under assumption control signal is constant during one switching period, discretized Eq. (19) with modeled computational delay is written as Eq. (20). Eq. (20) is written in “z” domain as Eq. (21).

$$z_2(n + 1) = z_2(n) + \int_{(n-1)T}^{nT} v dt \quad (20)$$

$$z_2 = \frac{T}{z(z-1)} v \quad (21)$$

Second integrator is written in integral form as Eq. (22). Discretized Eq. (22) is written as Eq. (23). Under assumption state z_2 changes linearly during one switching period, Eq. (23) is written in “z” domain as Eq. (24).

$$z_1(t - t_0) = z_1(t_0) + \int_{t_0}^t z_2(t) dt \quad (22)$$

$$z_1(n + 1) = z_1(n) + \int_{nT}^{(n+1)T} z_2(t) dt \quad (23)$$

$$z_1 = \frac{Tz+1}{2z-1} z_2 \quad (24)$$

Closed loop block diagram with discretized linearized KERS model and discrete PPI regulator is shown in Fig. 7. Proportional action in inner loop is displaced in feedback branch to obtain zero free transfer function. Regulator gains are normalized in Eq. (25). Transfer function in “z” domain with normalized gains is written as Eq. (26).

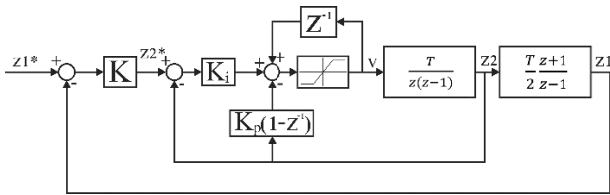


Fig. 7 Block diagram of regulator with anti-windup mechanism and displaced proportional action of inner loop.

$$i = TK_i; p = TK_p; pp = T^2KK_i \quad (25)$$

$$z_1(z) =$$

$$\frac{iz(z+1)}{z^4 - 3z^3 + (3+i+p+pp)z^2 - (1+i+2p-pp)z + p} z_1^*(z) \quad (26)$$

Eq. (27) defines criterion function as sum of regulator's error samples. If closed loop system has poles in segment $z_{pi} \in [0, 1]$ and no zeros, step response will be strictly aperiodic with no overshoot response. Then by minimizing criterion function, fastest strictly aperiodic response is obtained.

$$Q = \sum_{k=0}^{\infty} \Delta z_1(kT) \quad (27)$$

Minimizing criterion function [16] results in optimal regulator gains written as Eq. (28).

$$i = 0.056640625$$

$$pp = 0.001953125$$

$$p = 0.31640625 \quad (28)$$

Final regulator gains in Eq. (29) are five times smaller to obtain robust regulator.

$$K_i = \frac{i}{5T}; K_p = \frac{p}{5T}; K = \frac{2pp}{5T i}; \quad (29)$$

To obtain reference z_1^* , reference of DC link voltage u_c^* has to be non-linearly transformed to space of transformed states z_1 and z_2 . This transformation is written as Eq. (30).

$$z_1^* = \frac{1}{2} C u_c^{*2} + \frac{1}{2} L i^2 \quad (30)$$

To limit current of SC, reference z_2^* of inner control loop has to be limited. Current limits have to be transformed to space of transformed state z_1 and z_2 written as Eqs. (31) and (32). When SC voltage reaches maximum or minimum voltage, I_{max} value is changed as previously discussed.

$$z_{2min}^* = -E I_{max} - I_d u_c \quad (31)$$

$$z_{2max}^* = E I_{max} - I_d u_c \quad (32)$$

Anti-windup mechanism is shown in Fig. 7. Control signal is limited $u^* \in [0, 1]$. To limit control signal v , control signal u^* limits have to be transformed to space of states z_1 and z_2 , written as Eqs. (33) and (34).

$$v_{min} = \frac{E^2}{L} - \frac{I_d^2}{C} - \frac{E u_c}{L} - \frac{I_d i}{C} \quad (33)$$

$$v_{max} = \frac{E^2}{L} - \frac{I_d^2}{C} \quad (34)$$

7. Numerical Simulations

Computer numerical simulations were conducted in Matlab Simscape software package. Circuit from Fig. 2 was simulated for various torque profiles. Parameters of model are:

- $L = 10 \text{ mH}$ —inductor value;
- $R = 37 \text{ m}\Omega$ —inductor resistance;
- $C_{\text{DC_Link}} = 1,500 \text{ }\mu\text{F}$ —DC link capacitance;
- $\text{ESR}_{\text{DC_Link}} = 50 \text{ m}\Omega$ —equivalent series resistance of DC link capacitor;
- $C_{\text{Sup.Cap}} = 4 \text{ F}$ —supercapacitor capacitance;
- $R_{\text{Sup.Cap}} = 85 \text{ m}\Omega$ —supercapacitor internal resistance;
- $f_{\text{pwm}} = 10 \text{ kHz}$ —IGBT switching frequency;
- $\text{DeadTime} = 3 \text{ }\mu\text{s}$ —IGBT dead time;
- $f_s = 20 \text{ kHz}$ —sampling frequency of regulator;
- $I_{\text{max}} = 50 \text{ A}$ —maximum current of inductor and SC;
- $U_{\text{SCmax}} = 200 \text{ V}$ —SC maximum voltage;
- $U_{\text{SCmin}} = 120 \text{ V}$ —SC minimum voltage;
- $I_{\text{inverter_PEAK}} = 13 \text{ A}$ —peak value of inverter's output current;
- $\omega_1 = 600 \text{ rad/s}$ —low pass filter bandwidth in disturbance current estimator.

Results of the first simulation are shown on Fig. 8. First graph is inverter's current on DC side. Blue line is actual current and red line is estimated current. Second graph is DC link voltage. Third graph is SC voltage. Fourth graph is SC current. At first moment, inverter's current is positive, simulating motoring regime of drive and SC initial voltage is 150 V. When $t = 1 \text{ s}$, drive suddenly changes to generating mode, simulating braking. Inverter's current on DC side changes from maximum positive to maximum negative in 1 ms. Regulator suppresses disturbance of DC link voltage with overshoot of 1.6% in less than 16ms. This moment is shown in Fig. 9. When $t = 2 \text{ s}$, drive changes back to motoring mode in similar manner. When $t = 3 \text{ s}$, KERS is simulated in regime where inverter's current on DC side is changing in ramp. Inductor current ripple is less than 2% and DC link voltage ripple is less than 0.5%.

In the second simulation, shown in Fig. 10, robustness of regulator is tested. DC link has 10% smaller capacitance than capacitance parameter in regulator, thus simulating aging of device. KERS operates similar as in Fig. 8, but with slightly increased damped oscillations of SC current. At the end DC link working life, when capacitance drops 20%, SC current chatters and device operates with great losses.

Third simulation, shown in Fig. 11, simulates discharging of SC to minimum voltage, when drive is in motoring regime. When SC is discharged to minimum voltage, SC current limits in regulator are altered to prevent further discharge. At this moment, regulator is not able to keep DC link voltage at 600 V

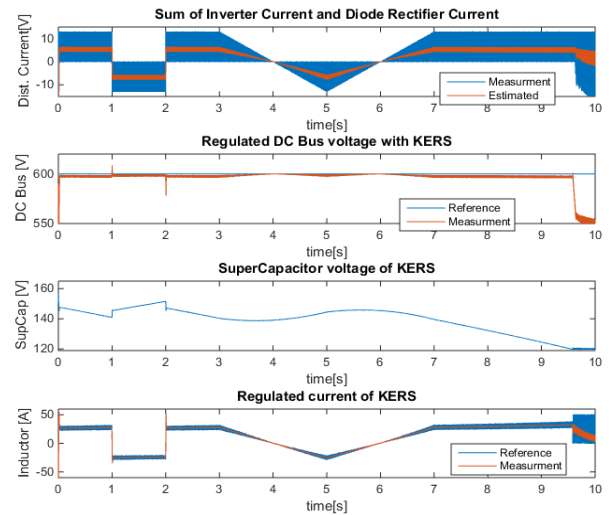


Fig. 8 Results of first simulation.

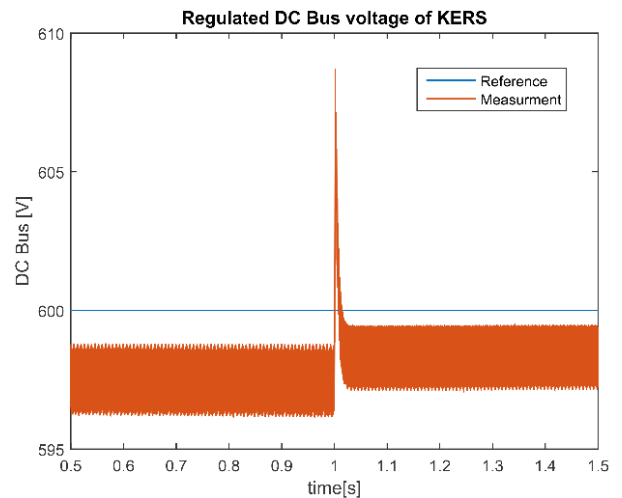


Fig. 9 DC link voltage disturbance when motor drive suddenly brakes.

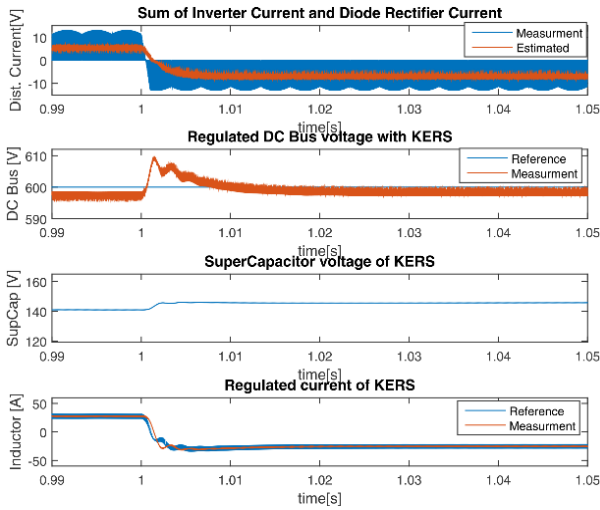


Fig. 10 Results of second simulation. DC link capacitance is reduced by 10%, simulating aging of device and testing robustness.

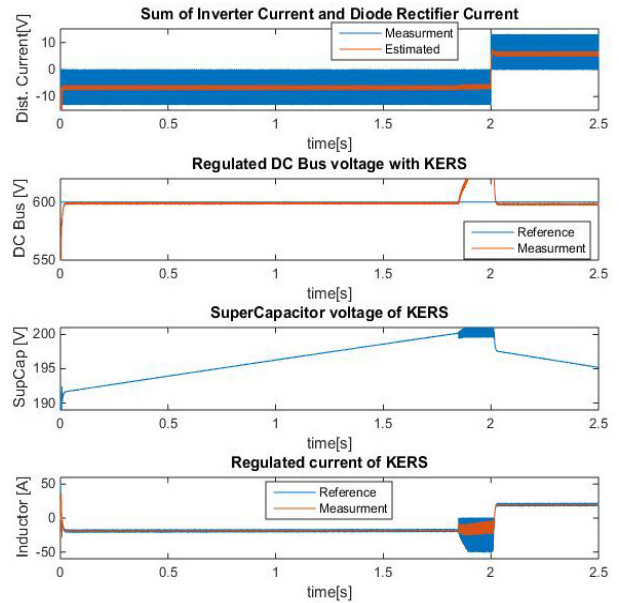


Fig. 12 Results of fourth simulation. SC charges to maximum voltage.

turned on. Later, motor drive changes to motor regime and DC link voltage stabilizes.

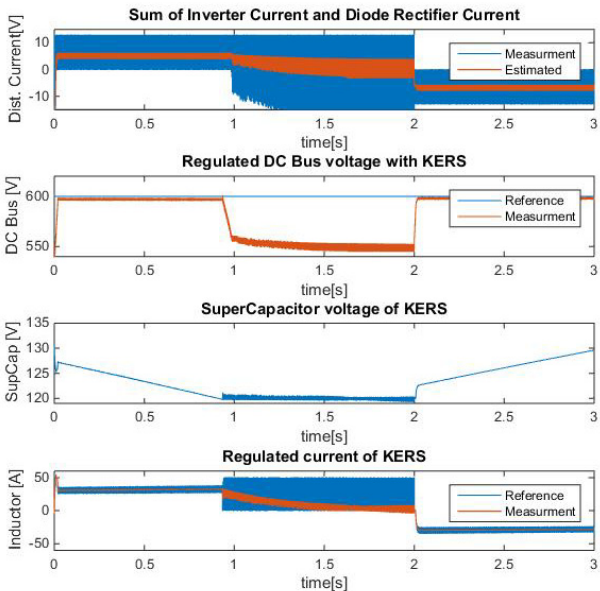


Fig. 11 Results of third simulation. SC discharges to minimum voltage. Later, at $t = 2$ s, motor drive brakes.

reference. DC link voltage drops and diode rectifier turns on. At this moment KERS operates with increased current ripple and transistors should be turned off.

In fourth simulation, overcharging of the SC is simulated. Results of fourth simulation are shown in Fig. 12. When SC voltage reaches maximum value, current limits in regulator are changed to prevent further charging of SC. As a consequence, DC link voltage increases. At this moment DBR should be

8. Conclusion

This paper presents a non-linear control algorithm for supercapacitor based non-isolated kinetic energy recovery system. It fulfils all KERS functionalities:

- Charging SC while motor drive is braking;
- Discharging SC while motor drive is accelerating;
- Limiting SC current and voltage;
- Stabilizing DC link voltage and suppressing sudden disturbances.

SC current ripple is less than 2% and DC link voltage ripple is less than 0.5%. Control algorithm relies only on two parameters; inductance of inductor and capacitance of DC link. SC capacitance is not parameter of regulator. Hence SC aging does not deteriorate performance of KERS. Regulator is able to suppress influence of rapidly changing torque on DC link voltage, relying on estimation of inverter's current on DC side. Control algorithm relies only on its own measurement, thus enabling KERS unit to be standalone device independent of motor drive.

References

- [1] Mittal, A. K., and Kumar, J. M. 2011. "Electrochemical Double-Layer Capacitors Featuring Carbon Nanotubes." *American Scientific Publishers, Encyclopedia of Nanoscience and Nanotechnology* 13: 263-71.
- [2] Conway, B. E. 2009. *Electrochemical Supercapacitor Scientific Fundamentals and Technological Application*. New York: Kluwer Academic/Plenum.
- [3] Beguin, F., and Frackowiak, E. 2001. "Carbon Materials for the Electrochemical Storage of Energy in Capacitors." *Carbon* 39: 937.
- [4] Francois, B. Raymundo-Pinjero, E., and Frackowiak, E. 2009. "Electrical Double-Layer Capacitors and Pseudocapacitors." *Carbons for Electrochemical Energy Storage and Conversion Systems*, Chapter 8. CRC Press, 329-75.
- [5] Goalous, H., Louahlia, H., and Gallay, R. 2011. "Supercapacitor Characterization and Thermal Modelling with Reversible and Irreversible Heat Effect." *IEEE Transaction on Power Electronics* 26 (11).
- [6] Maxwell 160V Module datasheet.
- [7] Vukosavić S. N. "Electrical Machines." *Power Electronics and Power System*, Springer.
- [8] Kim, S.-M., and Sul, S.-K. 2006. "Control of Rubber Tyred Gantry Crane with Energy Storage Based on Supercapacitor Bank." *IEEE Transactions on Power Electronics* 21 (5).
- [9] Azib, T., Bethoux, O., Remy, G., Marchand, C., and Berthelot, E. 2010. "An Innovative Control Strategy of a Single Converter for Hybrid Fuel Cell/Supercapacitor Power Source." *IEEE Trans. on Ind. El.* 57 (12).
- [10] Jabbour, N., and Mademlis, C. 2016. "Improved Control Strategy of a Supercapacitor Based Energy Recovery System for Elevator Applications." *IEEE Trans. Power Electron* 31 (12): 8398-408.
- [11] Jabbour, N., and Mademlis, C. 2017. "Supercapacitor-based Energy Recovery System with Improved Power Control and Energy Management for Elevator Applications." *IEEE Trans. Power Electron* 32 (12): 9389-99.
- [12] Ortuzar, M., Moreno, J., and Dixon, J. 2007. "Ultracapacitor-based Auxiliary Energy System for an Electric Vehicle: Implementation and Evaluation." *IEEE Trans. on Industrial Electronics* 54 (4).
- [13] Moreno, J., Ortuzar, M. E., and Dixon, J. W. 2006. "Energy-Management System for a Hybrid Electric Vehicle, Using Ultracapacitors and Neural Networks." *IEEE transactions on Industrial Electronics* 53 (2).
- [14] Payman, A., Pierfederici, S., and Meibody-Tabar, F. 2007. "Implementation of a Flatness Based Control for a Fuel Cell/Ultracapacitor Hybrid System." *Power Electronics Specialists Conference, IEEE*.
- [15] Becherif, M., Ayad, M. Y., and Miraoui A. 2006. "Modeling and Passivity-based Control of Hybrid Sources: Fuel Cell and Supercapacitors." *Industry Applications Conference, 2006. 41st Annual Meeting. Conference Record of the 2006 IEEE*.
- [16] Xu, N., and Riley, J. 2011. "Nonlinear Analysis of a Classical System: The Double Layer Capacitor." Elsevier B.V. *Electrochemistry Communication*. doi: 13, 10.1016/j.elecom.2011.07.003, 2011.
- [17] Zubieta, L., and Bonert, R. 2000. "Characterization of Double-Layer Capacitors for Power Electronics Applications." *IEEE Transactions on Industry Applications* 6 (1).
- [18] Vukosavić, S. N., Perić, L. S., and Levi, E. 2016. "A Three-Phase Digital Current Controller with Improved Performance Indices." *IEEE Transaction on Energy Conversion* 32 (1): 184-93.
- [19] Vukosavić, S. N. 2007. "Digital Control of Electrical Drives." *Power Electronics and Power System*. New York: Springer.